Overview of Small Fixed-Wing Unmanned Aircraft for Meteorological Sampling

JACK ELSTON, BRIAN ARGROW, MACIEJ STACHURA, DOUG WEIBEL, DALE LAWRENCE, AND DAVID POPE

University of Colorado Boulder, Boulder, Colorado

(Manuscript received 30 October 2013, in final form 10 July 2014)

ABSTRACT

Sampling the atmospheric boundary layer with small unmanned aircraft is a difficult task requiring informed selection of sensors and algorithms that are suited to the particular platform and mission. Many factors must be considered during the design process to ensure the desired measurement accuracy and resolution is achieved, as is demonstrated through an examination of previous and current efforts. A taxonomy is developed from these approaches and is used to guide a review of the systems that have been employed to make in situ wind and thermodynamic measurements, along with the campaigns that have employed them. Details about the airframe parameters, estimation algorithms, sensors, and calibration methods are given.

1. Introduction

Contemporary methods for atmospheric measurements, such as from towers and balloons, are limited in their ability to make targeted, in situ measurements of atmospheric phenomena (Giebel et al. 2012; Emeis et al. 2008; Foken and Nappo 2008). Manned aircraft have historically been used to fill many measurement gaps, and there are many examples of wind measurements from manned platforms for various applications (Lenschow 1972; Cho et al. 2003), including measurements in the hazardous environments of typhoons and hurricanes (Aberson and Franklin 1999), and supercell thunderstorms (Marwitz 1972). Safety and operational overhead usually dictate that manned aircraft must operate from airports, must fly with minimum altitude constraints, and must avoid hazardous conditions such as icing or severe turbulence.

Small unmanned aircraft systems (sUAS) provide instrument platforms able to operate in airspaces that are too difficult or hazardous for manned aircraft. Small UAS are typically much cheaper to construct, operate, and maintain than manned systems or larger UAS. This makes the loss of aircraft more acceptable in some high-risk applications. Furthermore, the simultaneous deployment of multiple aircraft for improved temporal (flight scheduling) or spatial (formation flying) measurements can be more feasible with relatively low-cost sUAS. Atmospheric sampling from small unmanned aircraft appears to date back to as early as 1961 (Konrad et al. 1970), with the first documented effort made in 1970 (Konrad et al. 1970). This aircraft made flights up to 3048 m and recorded dry-bulb temperature, wet-bulb temperature, relative humidity, pressure, airspeed, and vertical velocity of the aircraft.

Since then many sUAS platforms have been employed to measure meteorological phenomena. Giebel et al. (2012) provides an overview of currently available sensors, and a few of the sUAS platforms that have been used by the Risø National Laboratory for Sustainable Energy in a preliminary study on using sUAS atmospheric measurements in wind-power meteorology. Dias et al. (2012) summarize a study by the Simepar Technological Institute on high-resolution temperature and humidity measurements in the atmospheric boundary layer (ABL) and provide a comparison between several current platforms. Crowe et al. (2012) provides an overview of sUAS employed for Arctic environmental monitoring, including meteorology. Other groups have flown sUAS for meteorological applications, including the measurements of airmass boundaries (Houston et al. 2012), evaluating atmospheric models (Mayer et al. 2012c), sampling supercell thunderstorms (Elston et al. 2011), measurements of finescale turbulence (Balsley et al. 2012), and the verification of radar measurements (Chilson et al. 2009).

Corresponding author address: Jack Elston, Department of Aerospace Engineering Sciences, University of Colorado Boulder, 429 UCB, Boulder, CO 80309-0429.
E-mail: elstonj@colorado.edu

DOI: 10.1175/JTECH-D-13-00236.1

This paper provides a comprehensive overview of sUAS, where the use for atmospheric sampling has been reported, focusing on fixed-wing aircraft. A general characteristic of aircraft is that performance (speed, endurance, payload capacity) generally scales with physical dimensions. So, for a more specific comparison, the sUAS are subcategorized according to their general physical dimensions and performance. A survey of sensors that have been flown on specific platforms for in situ meteorological sensing is provided next with a comparison of measurement types, precisions, and accuracies. Sensors required for aircraft state estimation are also included in the survey. Regardless of the accuracy of an in situ sensor, high-precision measurements, especially for wind velocity, generally require an accurate aircraft state estimate for the transformation from the aircraft (body fixed) frame to the inertial (ground fixed) frame. It is therefore important to characterize the errors in the sensors used for the state estimates, which range from simple horizon-sensing thermopiles to high-precision accelerometers and gyros in an onboard inertial measuring unit (IMU). The choice and implementation of a filter algorithm to enhance the state estimate can be critical for accurate inertial wind-velocity measurements. A brief discussion of the importance of filter algorithms is presented that provides some background and criteria for making an informed filter choice. Finally, some important considerations for the sensor-platform airframe design are discussed, including influences of airframe components on integrated sensor calibration.

2. Small UAS employed for meteorological measurements

The following is an overview of several sUAS whose use for in situ meteorological sensing has been reported in the literature. They are separated into three categories based upon aircraft performance, payload capacity, and simplicity of operation (Fig. 1; Table 1). The first, category 1, where all vehicles have a weight of more than 10 kg and less than 30 kg, includes the Manta, ScanEagle, Aerosonde, and RPMSS. The category I sUAS provide the greatest payload capacity and endurance. Simply considering their relative size and weight, generally operating these larger aircraft requires the most operational overhead in terms of ground-based infrastructure and cost. The second sUAS category, category II, vehicles weigh between 1 and 10 kg and include the meteorological mini unmanned aerial vehicle (M^2AV), the multipurpose automatic sensor carrier (MASC), Tempest, University of Colorado Boulder NexSTAR, and the small multifunction autonomous research and teaching sonde (SMARTSonde). These sUAS lack the endurance and payload capacity of the category I aircraft but possess enough capacity to carry many of the atmospheric sensors used for wind measurements. Furthermore, their smaller physical size, and lower weight and cost make these aircraft easier to produce and operate. Weighing less than 1 kg, category III sUAS include the small unmanned meteorological observer (SUMO) and DataHawk, which have relatively smaller payload capacity and endurance than the other two categories, which reduces their ability to carry multiple sensors, and requires meteorological estimates to be made with less accurate sensors, or unique flight patterns and filtering algorithms. However, the trade-off in weight, cost, and size of these relatively small platforms enables data to be easily obtained by a user with little flight-related experience and allows the aircraft to be operated from almost anywhere with minimal logistical overhead.

a. Category I

1) CRUISER/CRYOWING

The Cruiser UAS has been employed both by the Norwegian Northern Research Institute (Norut), where it has been renamed the CryoWing, and by the Cyprus Institute for conducting atmospheric observations. Norut has modified the aircraft for use in Arctic campaigns, where it has been used to measure glacial ice, surface albedo (Bogren et al. 2011), and has made use of in situ measurements to determine the atmospheric effects on surface reflectance (Storvold et al. 2011). The Cyprus Institute is using the relatively large platform to host a variety of sensors in addition to the standard meteorological core for use in measuring radiative atmospheric properties, aerosols, and atmosphere dynamics (Lange et al. 2010).

2) UMARS

The unmanned modular airborne research system (UMARS) platform is a relatively new effort designed to provide a UAS specifically designed for atmospheric sampling that has a usable payload of up to 10 kg. The airframe features a modular payload bay that can be completely separated from the aircraft and has stable flight characteristics in turbulent environments. A sensor boom has been designed to be specifically used in conjunction with other scientific payloads, which includes a hygrometer, IMU, a thermocouple, and a multihole probe in one compact assembly. The vehicle has been test flown (Hesselbarth and Neininger 2013), but no use in meteorological campaigns has been documented.

3) MANTA

The BAE System's Manta has been used on several occasions by the Scripps Institution of Oceanography to conduct measurements of the atmosphere. In 2007 18

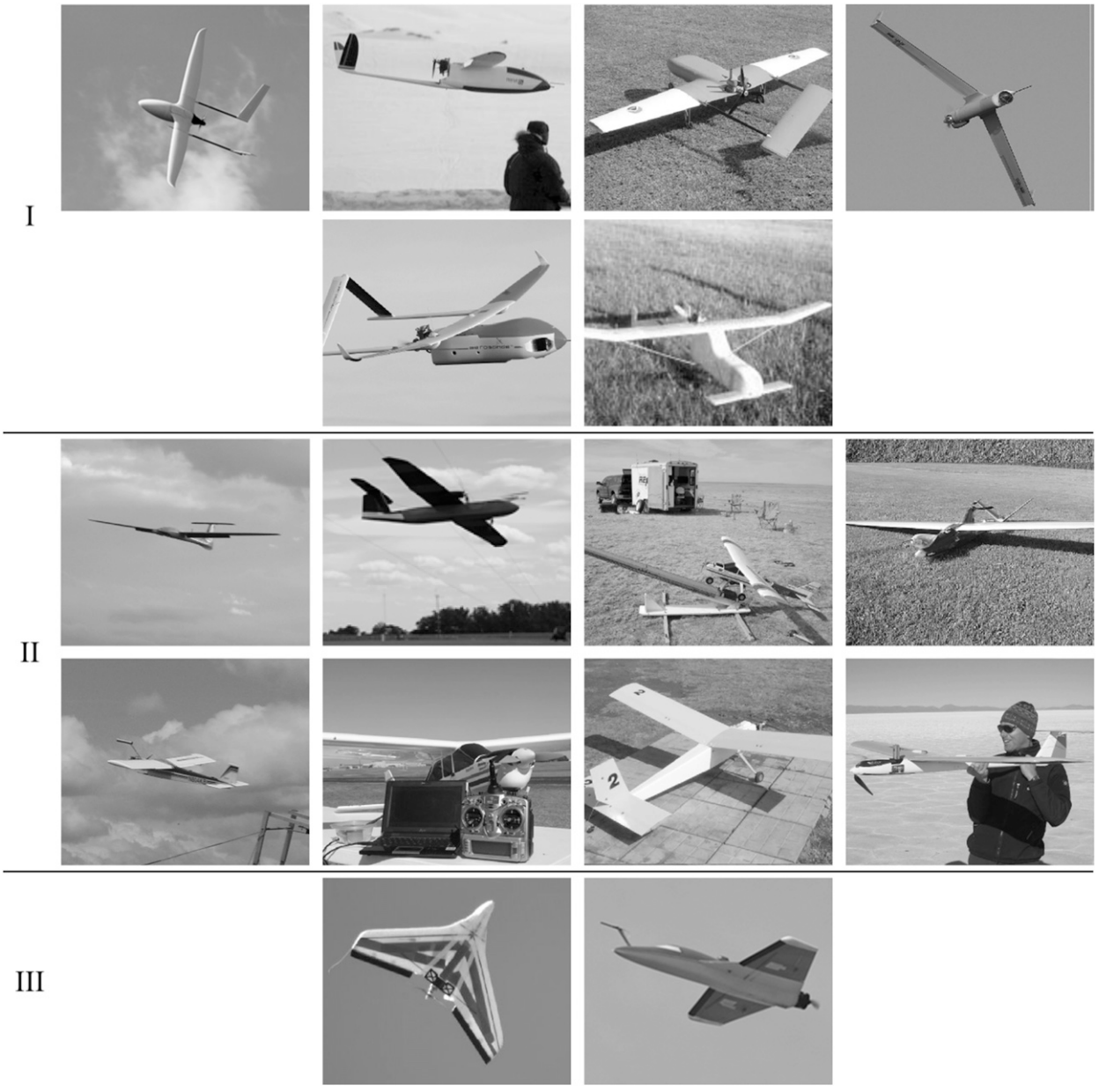

FIG. 1. The sUAS platforms for meteorological sampling of the ABL. (left to right, top to bottom) Category I: UMARS, Cruiser/CryoWing, Manta, ScanEagle, Aerosonde, RPMSS. Category II: Tempest, M^2AV, CU NexSTAR, MASC, Aerolemma-3, SMARTSonde, Powersonde, Kali. Category III: DataHawk, SUMO.

flights were conducted over the Indian Ocean to estimate the atmospheric solar heating caused by brown clouds (Ramanathan et al. 2007). In each mission, three vehicles were flown in a vertical stacked formation to simultaneously measure aerosol concentrations, soot amounts, and solar fluxes above, within, and below the clouds. More recently, the platform was used to measure momentum and heat fluxes in the ABL (Reineman et al. 2013). For this experiment, two instrument packages were designed for the Manta. One included fast-response turbulence, hygrometer, and temperature probes for momentum and heat flux measurements. The other payload included shortwave and longwave radiometers to determine surface temperature and albedo. Experiments were performed at Camp Roberts, California, to calibrate the instrumentation using ground-based sensors and to provide an atmospheric profile by flying in stacked formation. The Manta with the flux payload utilized measurements from a laser altimeter to maintain a constant 30-m offset from the ground, while the Manta with the

TABLE 1. Specifications of small UAS used in meteorological applications, with horizontal lines delineating the three categories of aircraft (categories I, II, and III). Maximum sampling altitude (AGL) is estimated or taken from the maximum reported height from flight experiments (Dias et al. 2012), which do not necessarily reflect system performance.

	UA	GTOW (kg)	Payload (kg)	Wingspan (m)	Endurance (min)	V_{cruise} (m s^{-1})	h^a_{max} (m)
I	Cruiser	35.0	6–10	3.8	360	33	5000
	UMARS 2	30.0	10.0	5.0	240	22	5000
	Manta	27.7	6.8	2.7	300	[23, 33]	5300
	ScanEagle	22.0	5.6	3.11	660	[28, 31]	4900
	Aerosonde	15.0	5.0	2.9	2400	[20, 32]	6000
	RPMSS	13.0	≈4.0	3.0	[240, 480]	≈25	5000
II	Tempest	3.2	2.2	6.8	90	25	1000
	M^{2}AV	5.6	1.5	2.0	45	22	2500
	CU NexSTAR	5.0	2.0	1.7	40	20	1000
	MASC	4.0	1.0	2.1	90	22	≈2500
	Aerolemma-3	≈3.6	1.2	1.2	15	17	2000
	SMARTSonde	3.5	≈1.0	1.7	25	[15, 20]	>300
	Powersonde	≈3.3	1.0	≈1	≈60	13	3000
	Kali	3.0	<0.6	2.1	≈15	≈20	4000
III	DataHawk	0.7	0.2	0.9	60	13	3000
	SUMO	0.58	0.14	0.8	30	15	3500

radiometric payload was commanded to fly directly overhead the first Manta at 178 m above the average surface altitude.

4) SCANEAGLE

An Insitu ScanEagle was outfitted by the Scripps Institution of Oceanography to perform measurements similar to the Manta, but over water (Reineman et al. 2013). Similar payloads were constructed to measure flux and radiation, and an additional payload was added to record visible and infrared imagery along with laser altimetry for ocean-surface topography. Calibration flights were performed in a similar manner to those conducted with the Manta, but with only one aircraft making short-duration (1–2 h) flights with each type of payload.

5) AEROSONDE

The Aerosonde was one of the first sUAS designed as a radiosonde and dropwindsonde replacement (Holland et al. (1992)). The platform provides unequaled endurance and range numbers (greater than 40 h and 4000 km), and when outfitted with two Vaisala RS90 sensor packages, the Aerosonde delivers meteorological results comparable to that of a traditional radiosonde (Soddell et al. (2004)). Aerosondes have been deployed successfully in a number of demanding meteorological campaigns (Holland et al. 2001), and its wind measurements have proven to be reasonably accurate, even in severe weather (Marks 2005).

6) RPMSS

The robotic plane meteorological sounding system (RPMSS) was designed by the China Meteorological Administration, and starting in 1992 it has provided targeted observations of the atmosphere without the spatial sampling limitations of a tethered balloon or balloon-based sonde (Shuqing et al. 2004). The platform has a proprietary meteorological suite and has been used in several field experiments; however, there are few published results from these experiments.

b. *Category II*

1) TEMPEST

The Tempest sUAS was designed by the Research and Engineering Center for Unmanned Vehicles (RECUV) at the University of Colorado Boulder and are specifically for use in sampling pretornadic and tornadic supercell thunderstorms (Elston 2011). The airframe is derived from competition slope-soaring, radio-controlled (RC) gliders, with a fuselage modified for electric propulsion, an avionics package that includes a Piccolo SL autopilot (Cloud Cap Technology), and payload. A Vaisala RS-92 probe is carried on the underside of the wing to measure pressure, temperature, and humidity (Roadman et al. 2012).

The Tempest sUAS was deployed in spring 2010 as part of the second Verification of the Origins of Rotation in Tornadoes Experiment (VORTEX2) and completed intercepts of six supercell thunderstorms (Roadman et al. 2012; Elston et al. 2011). It was deployed again in June 2013 in the Airdata Verification and Integrated Airborne Tempest Experiment (AVIATE) to verify airframe integration of an Aeroprobe Corporation five-hole air data probe with flights across and behind supercell gust fronts.

2) M^2AV

M^2AV was designed at the University of Braunschweig as a sUAS alternative to the manned helicopter-based Helipod meteorological sensing suite. The Helipod carries larger and significantly more accurate sensors; however, operational and airspace limitations that include flying under visual flight rules only, at prescribed minimum altitudes, coupled with the limited capability of the pilot to fly precise horizontal tracks, motivated the design of the M^2AV (Spieß 2006). To simplify operations, the relatively small Carolo T200 airframe manufactured by Mavionics GmbH (Buschmann et al. 2004) was selected for the M^2AV airframe. Its limited payload capabilities required a reduced sensor suite to be derived from the Helipod setup, which included the in-house manufacture and calibration of a five-hole probe.

The M^2AV sensor suite has demonstrated accuracy with extensive testing in a variety of experiments. Comparisons have been made against the Helipod (Spieß and Bange 2006), ground-based lidar (Spieß et al. 2007), and the wind measurements have been calibrated and compared to the combination of a meteorological tower and sodar (Van den Kroonenberg et al. 2008a). The M^2AV has also been deployed as a meteorological platform for various experiments (Van den Kroonenberg et al. 2008b); Martin et al. 2010), including campaigns in combination with other sUAS meteorological sensing platforms (Lothon et al. 2014; Giebel et al. 2012).

3) CU NexSTAR

The CU NexSTAR was deployed for airmass-boundary sampling experiments conducted during the 2009 Collaborative Colorado–Nebraska Unmanned Aircraft System Experiment (CoCoNUE). NexSTAR was developed by integrating a Cloud Cap Technology Piccolo Plus autopilot (Cloudcap; http://www.cloudcaptech.com/) into a Hobbico Inc. NexSTAR RC trainer kit airframe. The autopilot was used to augment the meteorological suite with its proprietary algorithm for wind estimation and was combined with two Vaisala RS-92 sondes installed in each wingtip to measure pressure, temperature, and humidity (Houston et al. 2012).

During the CoCoNUE experiment, the NexSTAR was flown over the Pawnee National Grassland in northeastern Colorado, where dual-Doppler wind measurements were made by the nearby Colorado State University–University of Chicago–Illinois State Water Survey (CSU-CHILL) and Pawnee Radar Facilities. The radar measurements generally agreed with the NexSTAR autopilot-derived estimates, and radar returns were also used to verify the relative position of UAS to meteorological phenomena, and confirmed that the aircraft transected a thunderstorm gust front (Houston et al. 2012).

4) MASC

The MASC was developed at the University of Tübingen (Giebel et al. 2012). Bungee launch and a removable payload section simplify operations, and a custom autopilot from the University of Stuttgart has been installed for semiautonomous flights. The current sensor package consists of the multihole probe used in the meteorological payload carried by the M^2AV, a custom thermocouple and thin-wire temperature measurement system, and a custom humidity sensor (Wildmann et al. 2013). This payload was carried by the MASC for ABL measurements in the Boundary Layer Late Afternoon and Sunset Turbulence (BLLAST) field campaigns (Wildmann 2011).

5) Aerolemma-3

The Aerolemma series of sUAS was designed by the Simepar Technological Institute in Brazil for routine, high-accuracy measurements of temperature and humidity on a fine vertical grid in the ABL. The original design employed a relatively large platform with an approximately 9-kg payload capability. It was outfitted with a sensor suite and flown with manual RC in 2006 and 2007 for ABL soundings. The installation was not properly vented, causing hysteresis in the data, and the manual piloting of the vehicle limited soundings to approximately 800 m AGL (Dias et al. 2009). A MicroPilot MP2028g autopilot was installed in the aircraft in an attempt to achieve soundings at higher altitudes, but the aircraft crashed shortly after takeoff. Some attempts to fly a second version of the original Aerolemma were made, but the airframe was determined to be too cumbersome for routine operations.

In 2009 a third design, Aerolemma-3 was created based on the Hobbico, Inc. Hobbistar 50 MK III kit. The use of the smaller, commercial airframe simplified construction, maintenance, and replacement. The HMP50 pressure and temperature sensor from the original Aerolemma platform was installed in a shrouded boom that placed them upstream of the nose-mounted propeller to reduce the effects of propeller wash on the instrumentation. A campaign was conducted with this platform in 2009 for continuous soundings over 3 days (Dias et al. 2012). Pressure, temperature, and humidity data from these flights were used to calculate potential virtual temperature profiles and entrainment fluxes.

6) SMARTSonde

Similar to the CU NexSTAR, the SMARTSonde airframe is developed from a modified Hobbico, Inc. NexSTAR RC trainer kit. The Paparazzi autopilot,

maintained by the École Nationale de l'Aviation Civile (ENAC), was employed with a Sensiron SHT75 sensor attached beneath the wing to measure temperature and humidity, and an SCP1000 sensor by VTI Technologies was mounted inside the fuselage for atmospheric pressure measurements (Chilson et al. 2009). Two-dimensional winds are estimated using successive GPS measurements (Bonin et al. 2013b), and an Aeroqual SM50 sensor was installed inside the fuselage to measure trace gases. Several flights were made to calibrate and verify measurements near the National Weather Center Mesonet tower in Norman, Oklahoma, in 2011 (Bonin et al. 2013a).

7) POWERSONDE

The Powersonde platform was developed as part of the National Oceanic and Atmospheric Administration (NOAA) glidersonde effort to create a reusable sonde for routine measurements of the atmosphere (Douglas 2008). Making the platform reusable had the advantages of reducing the cost of soundings and enabling the installation of expensive instruments whose one-time use in a standard dropsonde would be cost prohibitive. The glidersonde platform made use of balloon-borne launches to reach its maximum sampling altitude; however, helium can be difficult to obtain and transport, so a motor was added to create the Powersonde. This allowed for multiple soundings to be conducted up to 3-km altitude with an engine powered by gasoline, which is typically widely available. Lack of funding and Federal Aviation Administration (FAA) restrictions eventually forced the abandonment of this platform.

8) KALI

The Kali remote-control aircraft was designed to provide atmospheric soundings analogous to those provided by radiosondes while providing the ability to maintain station in high winds. The platform, built by Modellbau Ulrich and Blue Airlines, can be flown up to 4000 m AGL using specialized optics for the pilot. Kali did not provide wind measurements but was used successfully to collect meteorological data on the diurnal winds in the Kali Gandaki Valley in 2001 (Egger et al. 2002) and on the inflow onto the altiplano in the Bolivian Andes (Egger et al. 2005).

c. *Category III*

1) DATAHAWK

The DataHawk, originally developed at the University of Colorado Boulder for mobile networking experiments (Allred et al. 2007), is outfitted with temperature, pressure, and humidity sensors, and a 100-Hz cold-wire probe (Lawrence and Balsley 2013). The airframe is based on the commercially available Stryker RC aircraft and is similar to the FunJet platform employed by the SUMO UAS (described next). With its current propulsion system, the DataHawk can provide approximately 1-m resolution data from the surface to 2–3 km using a helical flight trajectory. Wind estimates are performed using sequential GPS speed-over-ground measurements. The DataHawk was used to gather meteorological data over the southern Peruvian coast in 2011 (Balsley et al. 2012) and has also been used to provide profiles to higher altitudes through deployment from a weather balloon (Lawrence and Balsley 2013). At the time of this writing, the DataHawk was being deployed near Oliktok Point, Alaska, as part of the Marginal Ice Zone Observations and Processes Experiment (MIZOPEX).

2) SUMO

The SUMO was designed by the University of Bergen and Martin Müller Engineering to provide a small, cost-effective tool for ABL research. It is based on the FunJet hobby kit manufactured by Multiplex Modellsport GmbH & Co. KG and is controlled using the Paparazzi autopilot (Reuder et al. 2009; Jonassen 2008). In its initial configuration, the platform was used to determine temperature and humidity using postprocessing to compensate for time lag in both sensors (Jonassen 2008), along with wind speed and direction using a "no-flow sensor" algorithm(Mayer 2011; Mayer et al. 2012a). This setup was validated during two field campaigns, one using intercomparisons between SUMO measurements and weather balloon soundings, and another using the combination of a tethersonde and the Kali sUAS (Jonassen 2008) for comparison.

The SUMO has been successfully used to provide data to compare to results from small-scale Weather Research and Forecasting (WRF) Model simulations in both Iceland and the Svalbard archipelago (Mayer et al. 2012c,b) and to provide ABL measurements in support of other Arctic research (Mayer et al. 2012b). The platform was recently modified to use an IMU rather than horizon-sensing thermopiles for a more accurate determination of state, and the meteorological sensors have been upgraded to include a faster response-time temperature sensor. For more accurate and higher-frequency wind measurements, an ETH Zürich seven-hole air data probe was integrated into the SUMO for wind-farm meteorology (Kocer et al. 2011), and an Aeroprobe Corporation five-hole air data probe for the BLLAST campaign (Reuder et al. 2012).

3. Sensor suite

Scientific measurement requirements that include type (wind, thermodynamic, species concentration, etc.),

TABLE 2. Small UAS used in meteorological applications and their sensors. CSI denotes Campbell Scientific Inc. NSSL denotes National Severe Storms Laboratory.

UA	Wind	Humidity	Temperature	Pressure
Cruiser	GP/IMU/ dynamic pressure	Varies	Varies	Varies
UMARS 2	Five-hole hemisphere	Thermocouple	Meteolabor AG "Snow White" dewpoint hygrometer	Measured around five-hole hemisphere
Manta	Nine-hole probe	Vaisala HMP45C	Vaisala HMP45C	All sensors barometric sensor
ScanEagle	Nine-hole probe	Vaisala HMP45C	Vaisala HMP45C	All sensors barometric sensor
Aerosonde	Proprietary algorithm	Vaisala RS90	Vaisala RS90	Vaisala RS90
RPMSS	GPS/INS	Humidity sensitive capacitor	Thermal resistor	MEMS
Tempest	Aeroprobe five-hole probe	Vaisala RS92	Vaisala RS92	Proprietary autopilot sensor
M^2AV	Five-hole probe	Vaisala HMP50	Vaisala HMP50 and thermocouple	Sensortechnics 144SC0811Baro
CU NexSTAR	Proprietary algorithm	Vaisala RS92	Vaisala RS92	Proprietary autopilot sensor
MASC	Five-hole probe	Custom (Wildmann et al. 2013)	Thin wire and thermocouple (Wildmann et al. 2013)	Sensortechnics 144SC0811Baro
Aerolemma-3	None	CSI HMP50	CSI HMP50	CSI CS100
SMARTSonde	GPS/infrared	Sensiron SHT75	Sensiron SHT75/VTI SCP1000	VTI SCP1000
Powersonde	None	NSSL Radiosonde	NSSL Radiosonde	NSSL Radiosonde
Kali	None	Honeywell HIH-3605-B	National Semiconductor LM50 C	Motorola MPX 2100
DataHawk	GPS/infrared	Honeywell capacitive polymer	TI ADS1118	MS5611–01BA03
SUMO	GPS/IMU	Sensiron SHT75	Sensiron SHT75 / PT1000	VTI SCP1000

location (ABL, tropical storm, etc.), and cadence (sample frequency, revisit rate, persistence, etc.) drive the selection of a sensor suite. Along with sensors specific to the meteorological application, as will be discussed in section 4, sensors for determining the aircraft's dynamic state are critical for atmospheric measurements, particularly wind velocity. Thus, one must have detailed knowledge about the sensors embedded in the avionics components that are often commercial-off-the-shelf (COTS) units running proprietary algorithms.

The following section describes the sensors that have been carried on the airframe platforms just described (Table 2) and that might be generally carried on sUAS dedicated to atmospheric sensing. Direct comparison of the measurement accuracies between the aforementioned categories of aircraft is difficult given the historical span of the missions and platforms considered here, and the continued improvement of accuracy and measurement frequency along with reduction of time constant in sensors. However, generally the aircraft with the larger payload capacity can carry a more accurate and diverse sensor payload. This can include improving measurements with the use of multiple sensors of a particular type, such as a fast-response, high-frequency sensor with low absolute accuracy that can be combined through a complementary filter with a low-frequency sensor with high absolute accuracy (Spieß 2006). It can also include instruments that provide an accurate instantaneous solution, such as a multihole probe for measuring wind velocity (Telionis et al. 2009) rather than estimating the wind indirectly through the combination of a dynamic model of the vehicle and GPS measurements (Mayer et al. 2012a). Although the smaller category III vehicles have included a multihole probe for wind and turbulence measurement (Reuder et al. 2012), such a large and heavy instrument mandates that smaller, less-accurate sensors are used for the other measurements to maintain appropriate flying weight and endurance.

a. *Wind and turbulence*

1) MULTIHOLE PROBE

Similar to a pitot-static probe, multihole probes provide measurements of stagnation and static pressure. They also contain a pattern of ports at different angles to the flow to allow for the determination of angle of attack α and sideslip β (Telionis et al. 2009). Recent developments in sensor technologies have reduced size and weight requirements for these units, and they have been employed on several small UAS to provide measurements of wind speed and direction (Van den Kroonenberg et al. 2008a; Kocer et al. 2011). Well-calibrated units can provide accurate measurements of flow angle up to 55° for five-hole probes and 75° for seven-hole probes (Mansour et al. 2011). They are typically tuned to provide the most accurate velocity estimates in the flight

regime of the aircraft, with the most common source of error being pressure waves within the tubing (Spieß 2006).

2) Pitot tube

Pitot tubes are standard sensors aboard fixed-wing aircraft to measure the indicated airspeed. These require the measurement of both stagnation pressure and static pressure. Stagnation pressure is measured at the tip of the pitot tube from a port oriented normal to the flow. Static pressure is either measured from ports located on the airframe or from ports on the side of the stagnation tube and parallel to the flow (a pitot-static probe). Bernoulli's equation is used to compute the flow speed from the difference of the stagnation and static pressures. Several miniature sensor options currently exist for measuring these pressures, usually trading cost and size for accuracy. Generally, the pressure sensors used for small pitot setups are more accurate at higher air speeds (with appropriate speed corrections to Bernoulli's equation), up to the saturation point of the sensors (Giebel et al. 2012).

3) Flush air sensing

Flush air sensing works on similar principles to the multihole probe; however, the pressure ports are integrated directly into the aircraft fuselage and then calibrated to measure α and β. These avoid the cost, difficulty of installation, and vibration and frequency response problems of typical boom-mounted setups (Kalogiros and Wang 2002b). Flush air sensing has been employed on a twin-jet manned aircraft (Tjernström and Friehe 1991), a Twin Otter (Kalogiros and Wang 2002b,a), and more recently on a small unmanned glider (Quindlen and Langelaan 2013).

4) Pressure strip

A novel method for airspeed and α measurement has been performed using a strip of inexpensive and lightweight pressure sensors (Callegari et al. 2006). Initial analysis shows the potential to make relatively accurate measurements using this method; however, no commercial system is readily available. Furthermore, no effort has been made to detect β using a similar method, although it appears to be possible.

5) α–β vanes

Angle-of-attack α and sideslip β measurements have also been made using vanes attached either to the aircraft fuselage or to a probe protruding into the free stream. These are typically not used in small UAS because of their fragile nature, increased drag, difficult construction, and relatively high cost.

6) Optical flow

An estimate of the aircraft angular or translational velocities can be determined through measuring the displacement of the surrounding environment between images made by a downward-facing camera. The technology may be considered a lower power and weight alternative to GPS, or an alternative in GPS-denied environments. It can also be used in combination with other sensors to determine aloft winds by calculating the difference between the optical flow angle and speed over ground (Moore et al. 2012).

Optical techniques for determining flow velocity include particle imaging velocimetry (PIV), particle tracking velocimetry (PTV), and schlieren photography. It appears, however, that none of the techniques has been used for directly sensing airborne particles for in situ measurements of flow velocity from a sUAS platform. Similar to the infrared sensors, this method is not subject to drift, but it is not yet versatile enough for general use as a navigation system in UAS and cannot be operated in low-visibility conditions.

7) Sonic anemometer

Sonic anemometers measure the slight changes in sound-propagation speed between a set of sensors in known locations to estimate the wind velocity. They have been tested on small, unmanned rotary aircraft, but most implementations are not small or light enough to be carried by sUAS (Giebel et al. 2012). One study has shown that winds can be derived using fixed-wing sUAS and ground-based emitters (Rogers and Finn 2013). Another preliminary study showed that a mass model of a sonic anemometer could be flown on a boom extending from the front of a sUAS, but experiments with the actual instrument have yet to be reported (Marques et al. 2013). Last, flight tests have been conducted with an Applied Technologies sonic anemometer for use in offshore wind and turbulence measurements, but no results have been published (Clarkson University UAV Team 2014).

b. Pressure

1) Pressure transducers

Microelectromechanical systems (MEMS) pressure sensors, commonly employed by sUAS, are generally based on measuring the strain on a diaphragm through resistive or capacitive changes in the material (Eaton and Smith 1997). They can be used in different configurations to provide absolute, gauge, or differential pressure measurements. Differential pressure is employed by multihole and pitot probe for measuring relative wind velocity. Absolute pressure not only provides

valuable information about the thermodynamic state of the atmosphere but it can also provide an accurate estimate of the relative height of the vehicle. To determine the absolute height of the vehicle, these pressure measurements have to be constantly calibrated to account for changes in the atmospheric pressure due to weather and temperature changes.

c. *Temperature and turbulence*

1) THIN-WIRE SENSORS

Thin-wire sensors are constructed from a thin wire filament supported under tension between prongs that hold the filament in the flow. The sensor operates on the principles of convective heat transfer that relate the instantaneous temperature difference between the air and the filament to the speed of the airflow over the filament. The temperature dependence of the filament's electrical resistance is used to generate an electrical output for an air-temperature or velocity-component measurement. The sensors are classified as a ''cold wire'' or a ''hot wire'' depending on whether the filament is actively heated, and they are further categorized as constant current, constant voltage, or constant temperature, based on the transducer circuitry design. Multisensor anemometry probes with three or four individual hot wires can be arranged onto a single probe to resolve three-dimensional flows (Jørgensen 2002; Singha and Sadr 2013).

Thin-wire probes (both cold and hot) are particularly effective for high-frequency turbulence measurements and have been used extensively for decades to produce accurate measurements of turbulence fluctuations. Balsley et al. (2012) report on the results of high-frequency cold-wire measurements from the DataHawk to investigate the ABL turbulence structure.

Although thin-wire probes have been used over a large flow-speed range (Comte-Bellot and Sarma 2001); Stainback and Nagabushana 1993), a major drawback for their use is their fragility. The thin wires and their support structures are relatively fragile and are prone to breakage from physical shock or the direct impact of particulates in the flow; thus, they are usually more suited to highly controlled wind-tunnel experiments than being mounted on a sUAS airframe, where robustness can be paramount.

2) THERMOCOUPLE

Thermocouple sensors utilize the principal that a metal wire subjected to a temperature gradient across its length will produce an electric potential. To measure this voltage, another wire must be connected to the point of measurement, known as the hot junction, and to a remote reference location called the cold junction. Using the same material for each wire will produce the same voltage between the hot junction and cold junction, and will not provide any measurable information about the relative temperature difference between the two points. However, different types of metals have a different relationship between temperature gradient and the induced voltage, so by using wires made of different materials, one can determine the relationship between the hot junction temperature and the voltage difference at the cold junction. This relationship is easily characterizable and repeatable across temperature cycles. The induced voltage does not rely on the length or size of the wires, making it possible to perform remote measurements.

A thermocouple by itself only provides the differential temperature between the hot junction and the cold junction. To measure the absolute temperature at the hot junction, a measurement of the absolute temperature of the cold junction must be performed and added to the differential temperature measurement. Wildmann et al. (2013) performed a comparison between a custom-built thermocouple and thin-wire probe. While both were able to meet the frequency, range, and accuracy requirements for use in sUAS for turbulent ABL measurements, the absolute measurement of the cold junction was most problematic when attempting to perform accurate total measurements.

3) SONIC ANEMOMETER

Already mentioned for their ability to measure wind velocity, sonic anemometers can simultaneously calculate the speed of sound along the sensor axes. From this, the sonic temperature, which has the same form as virtual temperature and is related to the density of the air, can be derived (Schotanus et al. 1983). The combined high-frequency measurement of wind and temperature allows for the calculation of temperature variance and sensible heat flux from a single instrument (Liu et al. 2001).

d. *Humidity*

HYGROMETER

Thin-film capacitive sensors are the most common method for measuring humidity on a small UAS. They consist of a porous dielectric that changes capacitance with changes in atmospheric water vapor and are usually coated to allow for the sensor to be completely immersed without sustaining irreversible changes. Thin-film capacitive sensors suffer from a dry bias at colder temperatures and have an exponentially increasing time constant with decreasing ambient temperatures. This constant is still relatively long for the environment commonly sampled with a sUAS, around 2–8 s for 20°C,

and up to tens of seconds for colder conditions, which makes it difficult to resolve thermodynamic properties of the atmosphere at small scales (Smit et al. 2013). Calibration of thin-film capacitive sensors before each flight is necessary because of the sensitivity to contamination, and many radiosondes employ a calibration process that removes the contamination by heating.

e. State and wind estimation

1) GPS

Small GPS units are generally combined with inertial or infrared sensors to provide an aircraft state estimate. This estimate is critical for converting aircraft-relative meteorological measurements to an inertial frame. Accuracy and measurement frequency of these units vary greatly, but they typically provide poor height estimates unless carrier-phase measurements are used. The best results are obtained through postprocessing, which can include historical atmospheric corrections. Furthermore, utilizing multiple antennas can provide an attitude estimate that is more accurate than current inertial navigation system (NS)/infrared sensor options available for sUAS (Evans et al. 1999).

GPS and vehicle orientation measurements can also be employed to perform wind estimation without any direct measurement of relative wind direction and magnitude (Soddell et al. 2004; Mayer et al. 2012a; Balsley et al. 2012; Langelaan et al. 2011; Roadman et al. 2012; Bonin et al. 2013b). Estimates made without a direct method for measuring aircraft-relative wind require fewer sensors and therefore can be implemented on a smaller, lighter, and cheaper airframe. However, a trade-off has to be made on the fidelity and frequency of the wind estimate, as these methods generally require an average wind vector to be determined over several successive measurements. Such an averaged estimate can be prone to error if the aircraft does not fly in a manner that makes the states observable, or if the algorithm fails to converge in the averaging time window. However, it can be a very useful tool for measuring slowly varying background winds, and some of the errors can be mitigated through the use of specific flight patterns.

2) INERTIAL SENSORS

Small MEMS inertial sensors are typically used in sUAS because of their low cost and weight. These sensors are less accurate than other inertial solutions, and the gyros are prone to drift. This can be compensated for by using various methods in the state estimate to compare to an inertial reference, such as a GPS or magnetometer. In the case of gyro measurements, the bias is strongly dependent on temperature, so the gyro should be calibrated before each flight with the knowledge that it can drift significantly during the duration of the aircraft's operation.

3) INFRARED SENSOR

A few sUAS utilize small infrared sensors to provide vehicle orientation relative to the horizon. These are usually less accurate than a short-term MEMS gyro solution and require calibration before flight, but they do not suffer from drift. They do, however, require a temperature difference between the ground and sky (a typical requirement is a difference of at least 8 K), which can limit their operations to areas without significant cloud cover (Mayer et al. 2012b).

4) MAGNETOMETER

One of the more difficult states to estimate is the heading angle ψ of the aircraft. Many systems assume that the aircraft is headed in the direction of the relative wind ($\beta = 0$), and estimate heading based on inertial measurements, a dynamic model of the system, and a comparison to GPS measurements. Unfortunately, this can be prone to large errors and requires the development of an accurate model of the aircraft. Small UAS that attempt to measure heading angle directly are forced to use differences in GPS carrier phase, or magnetometers. Measuring differences in GPS carrier phase requires a complex and expensive setup requiring multiple antennas and receivers, but they can provide a very accurate ψ estimate. Conversely, magnetometers are relatively inexpensive and easy to install but are generally inaccurate, as they suffer from interference from both external and local magnetic sources.

4. State estimation

State estimation is an often overlooked, but it is a critical component for making in situ measurements using a sUAS. For instance, a sensor may measure the wind velocity relative to the aircraft, but converting such a measurement to a measurement of the wind in the inertial frame requires information about the airframe velocity, attitude, and attitude rate. Often this information is obtained from autopilot output; however, depending on the autopilot's internal algorithms and quality of sensors, this can lead to significant induced errors in the converted measurements. Considering most sUAS airframes are passively stable, an autopilot can relax the accuracy requirements on the state estimation to reduce processor bandwidth and sensor cost while still being able to successfully control the aircraft.

To examine the source of measurement errors associated with state estimation, consider a wind sensor

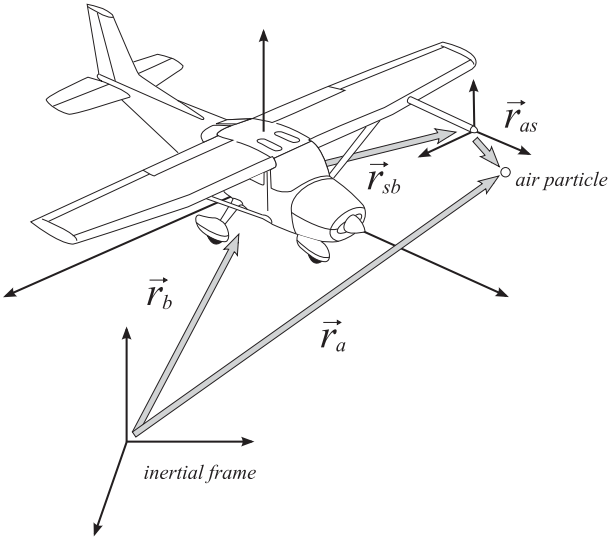

FIG. 2. Wind measurement geometry.

mounted to an airframe. Coordinate frames of interest are the inertial frame, body frame, and sensor frame, as shown in Fig. 2. The vector $\mathbf{r}_{as}$ describes the position of an air particle "observed" by the sensor and will have zero length for most sensors, but it is included for analysis, as it will have a nonzero timer derivative whenever the relative wind is nonzero. The quantity of interest, the velocity of the air particle relative to the inertial frame (i.e., the wind), is the time derivative of $\mathbf{r}_a$ with respect to the inertial frame, which can be expressed as

$$ {}^{I}\mathbf{v}_a = {}^{I}\frac{d}{dt}(\mathbf{r}_a) = {}^{I}\frac{d}{dt}(\mathbf{r}_b) + {}^{I}\frac{d}{dt}(\mathbf{r}_{sb}) + {}^{I}\frac{d}{dt}(\mathbf{r}_{as}), \quad (1) $$

where ${}^{I}(d/dt)(\cdot)$ denotes the time derivative taken with respect to the inertial frame, $\mathbf{r}_{sb}$ describes the sensor position and orientation relative to the body frame, $\mathbf{r}_b$ describes the position and orientation of the aircraft relative to the inertial frame, and ${}^{I}\mathbf{v}_a$ denotes the velocity of the air particle with respect to the inertial frame.

Assuming that the sensor is rigidly mounted, the vector $\mathbf{r}_{sb}$ is fixed in the body frame, but its time derivative in the inertial frame is nonzero if the airframe has a nonzero rotation rate. Considering the orientation and rotation of the body and sensor frames relative to the inertial frame, and assuming the sensor frame is oriented the same as the body frame, the wind in the inertial frame may be expressed as

$$ ({}^{I}\mathbf{v}_a)_I = ({}^{I}\mathbf{v}_b)_I + \mathbf{R}_I^b\left[({}^{I}\Omega_b)_b \times (\mathbf{r}_{sb})_b + ({}^{s}\mathbf{v}_a)_s\right], \quad (2) $$

where $({}^{I}\mathbf{v}_a)_I$ is the wind parameterized in the inertial frame, $({}^{I}\mathbf{v}_b)_I$ is the inertial velocity of the airframe, $\mathbf{R}_I^b$ is the inertial orientation of the airframe (rotation matrix), $({}^{I}\Omega_b)_b$ is the inertial rotation rate of the airframe parameterized in the body frame, $(\mathbf{r}_{sb})_b$ is the location of the sensor in the body frame, and $({}^{s}\mathbf{v}_a)_s$ is the relative wind or the velocity of the air in the sensor frame. This expression shows the explicit dependence of the wind measurement on the state of the airframe, in particular the velocity $[({}^{I}\mathbf{v}_b)_I]$, attitude $(\mathbf{R}_I^b)$, and attitude rate $[({}^{I}\Omega_b)_b]$. In addition, accurate determination of the location where each measurement was made is essential not only in converting the data to an inertial frame for comparison to other measurements and measurement sources but also significantly impacts the ability to accurately determine gradients and characterize features.

The airframe state, or elements of the state such as the attitude, may be estimated by several methods, including 1) sensors providing a direct measurement/estimate of some element of the state, for example, a Global Navigation Satellite System (GNSS) receiver providing a direct estimate of the location and velocity; 2) sensors whose measurement may be integrated to provide a measurement/estimate of some element of the state, for example, a three-axis gyroscope where the measured rotation may be integrated to yield attitude; or 3) a fusion of multiple sensors, such as an attitude and heading reference system where information from a three-axis gyroscope, accelerometer, and magnetometer is combined to yield attitude. Integration of sensor measurements, without sensor fusion, is generally impractical for sUAS, as sensors suitable for sUAS have noise and drift characteristics that cause an integrated value to diverge quickly. However, systems using direct measurements/estimation and sensor fusion have been employed for sUAS state estimation.

a. State estimation using direct measurements

The DataHawk is an example of a sUAS system using direct measurements for state estimation. The DataHawk employs horizon-sensing thermopiles to measure pitch and bank, with typical errors less than 5° for each axis. Yaw (compass heading) is measured with a two-axis magnetometer, with corrected estimates having accuracies within 5°. A GPS receiver is used to measure position and velocity, with the typical position and velocity estimate errors of 10 m and 0.2 m s^{-1}, respectively. The DataHawk does not estimate the full aircraft state; a gyroscope is not used to measure rotation rates, although one could be added to this system.

Direct measurement methods are almost always employed to measure one part of the state—the rotation rate. However, for other parts of the state, direct measurement methods generally yield inferior results to a sensor fusion method. Direct measurement of position

and velocity using a GNSS may be improved by fusing information from an accelerometer, particularly for high-frequency information. Direct measurement of attitude relies on measurement of two reference vectors, one of which is typically the local vertical. Local vertical may be measured with thermopiles, as employed in the DataHawk, or more commonly measured with an accelerometer. Unfortunately, thermopiles are difficult to calibrate and are affected by terrain and weather, and accelerometers measure specific force rather than gravity, and correcting for translational acceleration typically introduces significant errors. Fusing information from multiple sensors often allows for weaknesses of particular sensors to be overcome.

b. *Sensor fusion*

Sensor fusion approaches use a filter, or estimator, with these terms used interchangeably in this context, to combine information from multiple sensors to estimate (an element of) the aircraft state. The three most common filters employed in wind and state estimation for sUAS are the fixed gain observer (FGO) typically in the form of a complementary filter (CF); the Kalman filter (KF); and the extended Kalman filter (EKF), which is employed in lieu of the linear Kalman filter to handle nonlinear update equations. The complementary filter is mainly employed to estimate the attitude of the aircraft, while various forms of the KF and EKF are employed for estimating attitude and/or other states of the system. In addition to using different filter types, systems will differ in that some will use multiple filters, or filters and direct measurements, to estimate the full state as a combination of partial state estimates, while other systems will use a single filter to estimate the full state. Systems using multiple filters will often have a cascaded structure where the output of a first stage filter—for example, a filter estimating attitude—is used by a subsequent stage—for example, a stage employing integrated acceleration measurements to estimate velocity and position.

1) ATTITUDE ESTIMATION

Attitude estimation filters typically are based on integrating corrected gyroscope measurements where the correction signal is formed using accelerometer and magnetometer measurements to correct for zero-point drift in the gyroscope. The attitude state may be parameterized with Euler angles or a quaternion or rotation matrix. Attitude integration in three dimensions is a nonlinear function of rotation rate. Using discrete time gyroscope measurements, the attitude may be integrated using a first-order Euler method without incurring significant error when the gyroscope measurement rate is high. For lower measurement rates, more complex methods should be used (Savage 1998). Different filter types may use the same integration scheme but will differ in how the feedback correction signals are formed. For attitude estimation, each filter type has distinct advantages (Brown 1972). The CF can be used to estimate state over the operational envelope of the platform and is relatively computationally simple. An EKF is generally used for attitude estimation rather than a Kalman filter because of the inherent nonlinearity. The EKF, while generally more computationally costly than a CF, provides a more accurate estimate of the state, so long as it remains within a linearized regime. Remaining within the linearized regime is generally not an issue for wind measurement platforms, as most are flown in a docile manner for better wind estimation.

Conceptually, the complementary attitude filter integrates high-pass filtered gyro measurements and combines the resulting attitude estimate with a low-pass filtered attitude estimate based on an accelerometer measurement of the gravity vector and a magnetometer measurement of the earth's magnetic field vector. The high-pass and low-pass bands are chosen to be "complementary," so that the combined signal has unity gain across all frequencies. In practice a feedback structure is used to accomplish this with the gyroscope measurements being combined with a feedback (correction) signal based on the accelerometer and magnetometer measurements. Various schemes, based on gradient descent or other geometric constructions, have been used to form the feedback signals (Premerlani and Bizard 2009; Euston et al. 2009; Madgwick 2010). Proportional plus integral feedback is generally employed with the integrator states relating to, and compensating for, zero point bias drift in the gyroscope. Gains in a complementary filter are typically hand tuned. In some cases this can result in a frequency response that is not flat, so that the filter is not truly a complementary filter, but the filter may still be categorized as a fixed gain observer.

Feedback signals formed in FGOs using a gradient descent method or some geometric constructions or heuristic methods incorporate the observability of a particular state element by a particular sensor into the feedback gain, applying correction from that particular sensor to that particular state element. The EKF, while computationally more expensive than an FGO, provides a more accurate attitude estimate, as the feedback gains in an EKF depend not only on observability but on state estimate error covariance. By accounting for the uncertainty of sensor measurements in the state space, which includes both the sensor noise and the observability, and the uncertainty in the current state estimate, the EKF adjusts feedback gains applied to each sensor

measurement to be more appropriate than in an FGO. Another difference between CF/FGO and EKF attitude filters is that EKF attitude filters will include explicit states for the gyroscope bias (drift), while FGOs will incorporate proportional and integral feedback with the integrator states relating to the gyroscope biases. Numerous implementations of EKF attitude filters for sUAS can be found in the literature with Barton (2012) providing a pedagogical example.

2) VELOCITY AND POSITION ESTIMATION

A velocity- and position-estimating filter is often cascaded with an attitude filter. Accelerometer measurements may be integrated to yield velocity, which may be integrated to yield position. Attitude information is required as an input to this filter for two reasons:

- Accelerometers measure specific force on a proof mass, which is the difference between gravitational force on the proof mass and translational acceleration of the proof mass times its mass. The gravitational force may be removed from the measurement, using a priori knowledge of what the gravity force is in the inertial frame and the attitude information, so that the accelerometer may be used to measure acceleration.
- Measured acceleration is measured in the body frame, while it is desirable to parameterize velocity and position in the inertial frame. Attitude information is used to rotate acceleration or velocity and position from the body frame to the inertial frame.

Accelerometer measurements are typically available at a high rate providing for a high rate position and velocity estimate. Since estimation of velocity requires integration of the accelerometer measurement, noise in the measurements will cause the estimate to drift. Conversely, GPS measurements of position and velocity are not affected by drift, but are only available at low update rates (using low-cost, single-frequency receivers suitable for sUAS). Accelerometer and GPS measurements may be combined using sensor fusion. This could take the form of a CF, KF, or EKF.

If information from an airspeed sensor is incorporated into a velocity- and position-estimating filter, then the filter can estimate velocity, position, and mean wind speed.

3) OTHER FILTERS ESTIMATING PARTIAL STATE

While filters estimating attitude or velocity and position are common, filters estimating some other subset of the full state are also used in sUAS. For example, in the Paparazzi autopilot, the altitude P_d and the inertial vertical rate $\dot{P}_d$ are predicted using a KF. This filter fuses information from the z-axis accelerometer, a barometric pressure sensor, and GPS. A barometric pressure sensor may be used to estimate altitude based on the initial pressure at ground level and the hydrostatic decrease in atmospheric pressure with altitude. This provides a fast, high-resolution estimate of altitude, but the estimate is prone to drift due to normal weather-induced changes in ground-level atmospheric pressure. GPS provides an altitude estimate without drift, but with low accuracy and a low update rate. The filter state includes P_d and $\dot{P}_d$ as well as the bias in the barometric pressure sensor altitude estimate. The z-axis accelerometer measurement is integrated to yield altitude rate, which is integrated to yield altitude. Barometric pressure sensor and GPS measurements are used to correct the state estimate using the typical KF structure.

4) FULL STATE FILTERS

A single filter may be used to estimate the full state, including the attitude, attitude rate, position, and velocity. The estimated state may also include mean wind velocity and direction, gyroscope and accelerometer bias, barometric pressure sensor bias, etc. This approach has the advantage of potentially providing an optimal estimate of the full state. However, if the process model and sensor errors are not well known, and the filter must be tuned, then the large number of states can present difficulties.

Tuning issues can, to some extent, be circumvented by using an error state (or indirect) KF rather than an EKF. By estimating the error in the states rather than the states themselves, and by deriving the error state dynamics via the perturbation of the nonlinear plant, which will be linear, the conditions for (optimal) Kalman filtering are satisfied.

The M^2AV makes use of the error state KF for state estimation but includes GPS carrier-phase measurements. The combination of the IMU and GPS measurements provides significant accuracy improvements over an IMU-only system because of the complementary characteristics of each system (Van den Kroonenberg et al. 2008b). However, rather than use the GPS solution directly, a tightly coupled method is employed. This method generally uses an estimation of the distance to each satellite (called a pseudorange), the phase of the signal carrier wave, and the Doppler shift of the carrier. The Doppler shift is used to calculate the velocity of the satellite relative to the receiver (called the delta range). By using this raw information, the filter can be aided by GPS even when there are fewer than the four visible satellites required for a fix. It also maintains the accuracy of the location estimate while not requiring determination of the phasing integer ambiguities (van Graas and Farrell 2001). The 17 states used for the M^2AV error state filter are the position errors, velocity errors, orientation errors,

TABLE 3. State estimation methods used by sUAS for meteorological applications; unreported accuracies are left blank.

UA	Method	Error			
		Position (m)	Velocity ($m\,s^{-1}$)	Angle (heading; °)	Angular velocity ($deg\,s^{-1}\,Hz^{1/2}$)
Cruiser	Proprietary (Xsens MTI-G and Trimble BD982)	2.5	0.02	<0.5 (<1)	<0.15
UMARS 2	Complementary filter (Ardupilot)	Varies	Varies	Varies	Varies
Manta	Proprietary (NovAtel)	1.2	0.02	0.007 (0.011)	0.125
ScanEagle	Proprietary (NovAtel)	1.2	0.02	0.005 (0.007)	0.15
Aerosonde	Proprietary (Piccolo)	5.0	0.5	1.0 (2.4)	2.5
RPMSS	Proprietary				
Tempest	Proprietary (Piccolo)	5.0	0.5	1.0 (2.4)	2.5
M^2AV	Kalman filter			0.3 (0.5)	
CU NexSTAR	Proprietary (Piccolo)	5.0	0.5	1.0 (2.4)	2.5
MASC	Complementary filter (Paparazzi)	Varies	Varies	Varies	Varies
Aerolemma-3	Proprietary (MicroPilot)				
SMARTSonde	Complementary filter (Paparazzi)	Varies	Varies	Varies	Varies
Powersonde	None				
Kali	None				
DataHawk	Hybrid algorithm	10.0	0.2	5	
SUMO	Complementary filter (Paparazzi)	Varies	Varies	Varies	Varies

three gyro biases, three accelerometer biases, and the clock error and drift associated with the GPS.

c. *Implementations*

A number of the sUAS meteorology platforms use proprietary methods for obtaining state information (Manta, Scan Eagle, Aerosonde, CU NexSTAR, Tempest, RPMSS, Aerolemma). Although the methodology for state estimation in these units is generally unknown, the relative accuracy of the units is usually reported in the technical specifications. For the case of the M^2AV, the code base is proprietary, but some details are published about the state estimator, which utilizes a discrete error state KF (Vörsmann et al. 2012) to tightly couple GPS and INS measurements. On the opposite side of the spectrum open source solutions, such as the Paparazzi (Brisset et al. 2006) system, used for the SUMO, MASC, and SMARTSonde, publish their algorithms, making full analysis possible. The various known methods for state estimation that have been employed by autopilots for ABL sampling are tabulated in Table 3.

5. Calibration

Calibration for sUAS employed in making meteorological measurements consists of both sensor-based calibration, briefly mentioned in section 3, and system-level calibration. System-level calibration is necessary to remove the measurement errors caused by the construction and operation of the aircraft itself. For the M^2AV, for example, these errors were manifested as wind measurement errors on the order of $1\,m\,s^{-1}$ for each axis. They were discovered during a test flight that was made through an environment with a constant horizontal wind and near-zero vertical wind. During the flight it was observed that the vertical winds were not measured to be zero and that the horizontal wind measurements were dependent on flight direction.

To determine the source of the errors, an extensive error analysis was performed assuming nominal flight conditions. Given typical sensor measurement errors, a table was constructed defining the sensitivities of the inertial wind calculations to errors in each of the measurements (Van den Kroonenberg et al. 2008a). This analysis identified errors generated from mounting differences of the IMU and multihole probe, along with effects on the measured airspeed from the fuselage, wings, and propulsion that were not included in the wind tunnel calibration of the multihole probe (due to the size of the tunnel). The effect of the roll-axis errors were negligible, leaving three parameters to be determined: the pitch and yaw differences between the IMU and air data axis, $\Delta\phi'$ and $\Delta\psi'$ respectively; and a scaling factor for the observed relative wind speed, f_{U_a}, used to account for differences from the wind tunnel calibration. By performing a flight test in conditions where it is safe to assume near-zero vertical winds and identical horizontal wind components between two coincident flight legs in opposite directions, these unknown parameters were estimated by comparing measurement differences over both passes.

Other system-level calibration errors include dealing with time constants of the sensors. Preliminary work with the SUMO system revealed a disagreement

between temperature and humidity measurements between ascending and descending profiles (Jonassen 2008). This was attributed to the time constants of each sensor and was more apparent on the ascending profile, where the vertical speed was larger than on the descent. An algorithm was created to estimate the time constants that were applied in postprocessing and showed good agreement with balloon-borne radiosonde soundings (Jonassen 2008).

Comparison flights have been performed against other well-established measurement methods to provide a reference for calibration. One of the first examples was the comparison of data from a balloon-borne radiosonde and the Aerosonde UAS (Soddell et al. 2004). Since then, several efforts have been carried out to compare measurements made by sUAS to tethered kites (Mayer et al. 2012b), balloon-borne radiosondes (Soddell et al. 2004), sodar and lidar installations (Spieß 2006), instrumented towers (Van den Kroonenberg et al. 2008a), and against other sUAS measurements (Wildmann 2011). Generally, good agreement between the types of measurement is demonstrated, although the limited spatial and temporal resolution of some of the legacy sensing systems makes it difficult to conduct accurate intercomparisons.

6. Regulatory requirements

There is increasing international pressure on civil aviation authorities to integrate UAS into the airspaces around the world. The International Civil Aviation Organization (ICAO) is working to harmonize emerging rules and policies for UAS operations (ICAO 2011). In the United States, the Federal Aviation Administration Modernization and Reform Act of 2012 mandated that the FAA develop a plan to safely integrate UAS into the national airspace system (NAS) by 30 September 2015 (U.S. House of Representatives 2012, sections 331–336).

In the United States, aircraft are categorized as civil (associated with commercial ownership or activities) or public (associated with government ownership or activities). An experimental airworthiness certificate is required to operate a civil UAS, while a Certificate of Waiver or Authorization (COA) is required to operate a UAS in the public category. Public proponents can ''self-certify'' the airworthiness of their UAS. The self-certification policy has proven to be less onerous than the requirement for the experimental certificate. Consequently, most ''legal'' operations of sUAS in the United States have been conducted by public entities, such as government and law enforcement agencies, and public universities. A FAA rule to regulate the operations of small sUAS [<55 lb (25 kg)] in the NAS is pending. Based on recommendations published in 2009 by the FAA's Small Unmanned Aircraft System Aviation Rulemaking Committee (Tarbert and Wierzbanowski 2009), it is expected that the final sUAS rule will allow operations similar to those currently allowed by the FAA guidelines for a hobbyist operating model aircraft (van Vuren 1981). It is expected that operations that exceed the constraints of the new sUAS rule will continue with the current policies for civil and public UAS operations.

7. Summary

There is a large body of work describing meteorological sampling using sUAS over a range of applications. Many have been summarized in this article, along with design and operational details. From the multitude of approaches, it is evident that meteorological sampling is more difficult than might be assumed, and that is requires a careful combination of platforms, sensors, algorithms, and a concept of operations specific to the needs of the application.

Platform selection starts with the measurement requirements and the required positioning of sensors. Pressure and velocity measurements are directly influenced by the distortion of the flow field from the airframe and probes to support sensors. Temperature, humidity, and species concentration measurements are potentially influenced by the energy transfer (heat) from the airframe, particularly motors, engines, and exhaust streams. Sensors such as radiometers may require unrestricted views of the horizon, zenith, and/or nadir. These influences on measurements are called out separately for illustrative purposes; however, their affects are almost always coupled.

The selection or design process must address the aircraft performance requirements, which are directly driven by the scientific application and sampling strategy. These include the traditional measures of aircraft performance—that is, maximum takeoff weight, takeoff and landing performance, range, endurance, altitude, and rate of climb. The size and form factor of the avionics and sensor payloads directly drive the volumetric sizing, and the weight and balance of the airframe. Generally, the more integrated the airframe and sensors, the less flexibility there is for alternatives.

Strategy and the needs of the application also drive the accuracy and type of sensors. Critical parameters are accuracy, time constant, and measurement frequency, along with cost, weight, and volume. For more expensive sUAS with larger payloads, as was demonstrated in the M^2AV work (Van den Kroonenberg et al. 2008b), two

sensors with complementary characteristics have been combined to deal with the common issue of the time constant and accuracy trade-off. A filter is generally used to combine higher-frequency measurements prone to drift with accurate measurements that have long time constants. For smaller platforms where such a sensor suite is too large and heavy, other techniques are be available, such as comparing differences between the ascent/descent or legs of a flight pattern conducted in opposite directions to remove errors from drift or long time constants. The ability to compensate for a limited sensor suite should also be considered. In these cases, lack of information—for instance, the measurement of the magnetic field or side-slip angle—will require assumptions, such as that the heading of the vehicle has a constant offset into the relative winds for the entire flight regime during an averaged measurement (Mayer et al. 2012a; Bonin et al. 2013a; Lawrence and Balsley 2013). Depending on the platform and the accuracy required, this lack of information may be acceptable.

Finally, the correct algorithm should be selected for the fidelity and resolution required by the application. Given the typical sensor suite used on a sUAS, the best algorithm to account for the main sources of error must account for sensor bias and drift. Algorithms such as variants of the KF are able to accomplish this task and will be more accurate than simple curve fits based on a small set of data points. Care must also be taken to select algorithms that consider the effects of parameters such as centripetal acceleration to avoid, for instance, inaccurate wind estimation during coordinated turns. This can be performed on computationally limited sensor packages by recording the data for postprocessing. The autopilot may not need a high-quality attitude estimate to adequately fly the aircraft, so a simple attitude filter can be used in the autopilot while a more complicated filter, possibly requiring relatively high computational power, can be used in postprocessing. As demonstrated by the SUMO (Mayer et al. 2012a) and SMARTSonde (Bonin et al. 2013a), postprocessing the data improves the accuracy of estimates based on the measured values, including those of the aloft winds (Khelif et al. 1999).

Acknowledgments. This material is based upon work supported by the National Science Foundation under Award AGS-1231096.

REFERENCES

Aberson, S. D., and J. L. Franklin, 1999: Impact on hurricane track and intensity forecasts of GPS dropwindsonde observations from the first-season flights of the NOAA Gulfstream-IV jet aircraft. *Bull. Amer. Meteor. Soc.,* **80,** 421–427, doi:10.1175/1520-0477(1999)080<0421:IOHTAI>2.0.CO;2.

Allred, J., and Coauthors, 2007: Sensorflock: An airborne wireless sensor network of micro-air vehicles. *SenSys '07: Proceedings of the Fifth International Conference on Embedded Networked Sensor Systems,* ACM, 117–129.

Balsley, B. B., D. A. Lawrence, R. F. Woodman, and D. C. Fritts, 2012: Fine-scale characteristics of temperature, wind, and turbulence in the lower atmosphere (0–1, 300 m) over the south Peruvian coast. *Bound.-Layer Meteor.,* **147,** 165–178, doi:10.1007/s10546-012-9774-x.

Barton, J. D., 2012: Fundamentals of small unmanned aircraft flight. *Johns Hopkins APL Tech. Dig.,* **31,** 132–149.

Bogren, W. S., J. F. Burkhart, R. Storvold, S. Solbø, and VAUUAV Science Team, 2011: Cryowing in VAUUAV: Performance assessment of reflectance measurements from an unmanned aerial platform. *2011 Fall Meeting,* San Francisco, CA, Amer. Geophys. Union, Abstract C51A-0637.

Bonin, T., P. Chilson, B. Zielke, and E. Fedorovich, 2013a: Observations of the early evening boundary-layer transition using a small unmanned aerial system. *Bound.-Layer Meteor.,* **146,** 119–132, doi:10.1007/s10546-012-9760-3.

——, ——, ——, P. Klein, and J. Leeman, 2013b: Comparison and application of wind retrieval algorithms for small unmanned aerial systems. *Geosci. Instrum., Methods Data Syst.,* **2,** 177–187, doi:10.5194/gi-2-177-2013.

Brisset, P., A. Drouin, M. Gorraz, P.-S. Huard, and J. Tyler, 2006: The paparazzi solution. *Proc. 2nd US-European Competition and Workshop on Micro Air Vehicles (MAV2006),* Sandestin, Florida, École Nationale de l'Aviation Civile. [Available online at https://hal-enac.archives-ouvertes.fr/hal-01004157/document.]

Brown, R. G., 1972: Integrated navigation systems and Kalman filtering: A perspective. *Navigation,* **19,** 355–362, doi:10.1002/j.2161-4296.1972.tb01706.x.

Buschmann, M., J. Bange, and P. Vörsmann, 2004: MMAV—A miniature unmanned aerial vehicle (mini-UAV) for meteorological purposes. *16th Symp. on Boundary Layers and Turbulence,* Portland, ME, Amer. Meteor. Soc., 6.7. [Available online at https://ams.confex.com/ams/BLTAfIRSE/techprogram/paper_77875.htm.]

Callegari, S., M. Zagnoni, A. Golfarelli, M. Tartagni, A. Talamelli, P. Proli, and A. Rossetti, 2006: Experiments on aircraft flight parameter detection by on-skin sensors. *Sens. Actuators,* **130–131A,** 155–165, doi:10.1016/j.sna.2005.12.026.

Chilson, P. B., and Coauthors, 2009: SMARTSonde: A small UAS platform to support radar research. *34th Conf. on Radar Meteorology,* Williamsburg, VA, Amer. Meteor. Soc., 12B.6. [Available online at https://ams.confex.com/ams/34Radar/techprogram/paper_156396.htm.]

Cho, J. Y. N., R. E. Newell, B. E. Anderson, J. D. W. Barrick, and K. L. Thornhill, 2003: Characterizations of tropospheric turbulence and stability layers from aircraft observations. *J. Geophys. Res.,* **108,** 8784, doi:10.1029/2002JD002820.

Clarkson University UAV Team, cited 2014: Clarkson University's unmanned aerial vehicle ''Golden Eagle'' project. [Available online at http://clarksonuniversityuav.blogspot.dk.]

Comte-Bellot, G., and G. R. Sarma, 2001: Constant voltage anemometer practice in supersonic flows. *AIAA J.,* **39,** 261–270, doi:10.2514/2.1321.

Crowe, W., and Coauthors, 2012: Enabling science use of unmanned aircraft systems for Arctic environmental monitoring. Arctic Monitoring and Assessment Programme Tech. Rep. 6, 30 pp.

Dias, N. L., J. E. Gonçalves, A. L. Malheiros, and T. Hasegawa, 2009: Probing the atmospheric boundary-layer with a cost-effective mini-UAV. *AsiaFlux Newsletter,* No. 30, Seoul, South Korea, AsiaFlux, 16–22.

——, ——, L. Freire, T. Hasegawa, and A. Malheiros, 2012: Obtaining potential virtual temperature profiles, entrainment fluxes, and spectra from mini unmanned aerial vehicle data. *Bound.-Layer Meteor.,* **145,** 93–111, doi:10.1007/s10546-011-9693-2.

Douglas, M., 2008: Progress towards development of the glidersonde: A recoverable radiosonde system. Preprints, *WMO Tech. Conf. on Meteorological and Environmental Instruments and Methods of Observation (TECO-2008),* St. Petersburg, Russia, WMO, P1(6). [Available online at http://www.knmi.nl/samenw/geoss/wmo/TECO2008/IOM-96-TECO2008/P1(06)_Douglas_USA.pdf.]

Eaton, W. P., and J. H. Smith, 1997: Micromachined pressure sensors: Review and recent developments. *Smart Mater. Struct.,* **6,** 530, doi:10.1088/0964-1726/6/5/004.

Egger, J., and Coauthors, 2002: Diurnal winds in the Himalayan Kali Gandaki Valley. Part III: Remotely piloted aircraft soundings. *Mon. Wea. Rev.,* **130,** 2042–2058, doi:10.1175/1520-0493(2002)130<2042:DWITHK>2.0.CO;2.

——, and Coauthors, 2005: Diurnal circulation of the Bolivian Altiplano. Part I: Observations. *Mon. Wea. Rev.,* **133,** 911–924, doi:10.1175/MWR2894.1.

Elston, J. S., 2011: Semi-autonomous small unmanned aircraft systems for sampling tornadic supercell thunderstorms. Ph.D. thesis, University of Colorado, 293 pp. [Available online at http://gradworks.umi.com/34/53/3453706.html.]

——, J. Roadman, M. Stachura, B. Argrow, A. Houston, and E. W. Frew, 2011: The tempest unmanned aircraft system for in situ observations of tornadic supercells: Design and VORTEX2 flight results. *J. Field Rob.,* **28,** 461–483, doi:10.1002/rob.20394.

Emeis, S., K. Schäfer, and C. Münkel, 2008: Surface-based remote sensing of the mixing-layer height—A review. *Meteor. Z.,* **17,** 621–630, doi:10.1127/0941-2948/2008/0312.

Euston, M., P. Coote, R. Mahony, J. Kim, and T. Hamel, 2009: A complementary filter for attitude estimation of a fixed-wing UAV. *2008 IEEE/RSJ International Conference on Intelligent Robots and Systems,* IEEE, 340–345.

Evans, J., W. Hodge, J. Liebman, C. J. Tomlin, and B. Parkinson, 1999: Flight tests of an unmanned air vehicle with integrated multi-antenna GPS receiver and IMU: Towards a testbed for distributed control and formation flight. *Proceedings of the 12th International Technical Meeting of the Satellite Division of the Institute of Navigation (ION GPS 1999),* ION, 1799–1808.

Foken, T., and C. J. Nappo, 2008: *Micrometeorology*. Springer, 308 pp.

Giebel, G., U. Schmidt Paulsen, J. Bange, A. la Cour-Harbo, J. Reuder, S. Mayer, A. van der Kroonenberg, and J. Mølgaard, 2012: Autonomous aerial sensors for wind power meteorology—A pre-project. Danmarks Tekniske Universitet, Risø Nationallaboratoriet for Bæredygtig Energi Rep., 90 pp.

Hesselbarth, H., and B. Neininger, 2013: UAV-platform UMARS 2 for environmental research. *First Conf. of the Int. Society for Atmospheric Research Using Remotely-Piloted Aircraft,* Palma de Mallorca, Balearic Islands, Spain. [Available online at http://www.cost-uas.net/fileadmin/user_upload/infos/Meetings/Meeting_Palma_20120218/ISARRA_Conference/Session_1/UMARS_ISARRA_COST2013.pdf.]

Holland, G. J., T. McGeer, and H. Youngren, 1992: Autonomous aerosondes for economical atmospheric soundings anywhere on the globe. *Bull. Amer. Meteor. Soc.,* **73,** 1987–1998, doi:10.1175/1520-0477(1992)073<1987:AAFEAS>2.0.CO;2.

——, and Coauthors, 2001: The aerosonde robotic aircraft: A new paradigm for environmental observations. *Bull. Amer. Meteor. Soc.,* **82,** 889–902, doi:10.1175/1520-0477(2001)082<0889:TARAAN>2.3.CO;2.

Houston, A., B. Argrow, J. Elston, J. Lahowetz, and P. Kennedy, 2012: The collaborative Colorado–Nebraska unmanned aircraft system experiment. *Bull. Amer. Meteor. Soc.,* **93,** 39–54, doi:10.1175/2011BAMS3073.1.

ICAO, 2011: Unmanned aircraft systems (UAS). International Civil Aviation Organization Tech. Rep., Cir 328, AN/190, 38 pp. [Available online at http://www.icao.int/Meetings/UAS/Documents/Circular%20328_en.pdf.]

Jonassen, M. O., 2008: The small unmanned meteorological observer (SUMO): Characterization and test of a new measurement system for atmospheric boundary layer research. M.S. thesis, Meteorology, Geophysical Institute, University of Bergen, 125 pp. [Available online at http://www.uib.no/sites/w3.uib.no/files/w2/ma/master_jonassen.pdf.]

Jørgensen, F. E., 2002: 9040U6151. How to measure turbulence with hot-wire anemometers—A practical guide. Dantec Dynamics A/S Publ. 9040U6151, 73 pp.

Kalogiros, J. A., and Q. Wang, 2002a: Aerodynamic effects on wind turbulence measurements with research aircraft. *J. Atmos. Oceanic Technol.,* **19,** 1567–1576, doi:10.1175/1520-0426(2002)019<1567:AEOWTM>2.0.CO;2.

——, and ——, 2002b: Calibration of a radome-differential GPS system on a Twin Otter research aircraft for turbulence measurements. *J. Atmos. Oceanic Technol.,* **19,** 159–171, doi:10.1175/1520-0426(2002)019<0159:COARDG>2.0.CO;2.

Khelif, D., S. P. Burns, and C. A. Friehe, 1999: Improved wind measurements on research aircraft. *J. Atmos. Oceanic Technol.,* **16,** 860–875, doi:10.1175/1520-0426(1999)016<0860:IWMORA>2.0.CO;2.

Kocer, G., M. Mansour, N. Chokani, R. Abhari, and M. Müller, 2011: Full-scale wind turbine near-wake measurements using an instrumented uninhabited aerial vehicle. *J. Sol. Energy Eng.,* **133,** 041011, doi:10.1115/1.4004707.

Konrad, T. G., M. L. Hill, J. R. Rowland, and J. H. Meyer, 1970: A small, radio-controlled aircraft as a platform for meteorological sensors. *Johns Hopkins APL Tech. Dig.,* **10,** 11–21.

Lange, M., A. Teller, C. Keleshis, S. Ioannou, P. Philimis, J. Lelieveld, and Z. Levin, 2010: Autonomous Flying Platforms for Atmospheric and Earth Surface Observations (APAESO)—A pioneering research facility in Cyprus. *Geophysical Research Abstracts,* Vol. 12, Abstract 8137. [Available online at http://meetingorganizer.copernicus.org/EGU2010/EGU2010-8137-1.pdf.]

Langelaan, J. W., N. Alley, and J. Neidhoefer, 2011: Wind field estimation for small unmanned aerial vehicles. *J. Guid. Control Dyn.,* **34,** 1016–1030, doi:10.2514/1.52532.

Lawrence, D. A., and B. B. Balsley, 2013: Design of a low-cost UAS for high-resolution atmospheric sensing. *Proceedings of the AIAA Infotech@Aerospace Conference,* American Institute of Aeronautics and Astronautics, 566–567, doi:10.2514/6.2013-4669.

Lenschow, D., 1972: The measurement of air velocity and temperature using the NCAR Buffalo aircraft measuring system. NCAR Tech. Rep. NCAR-TN/EDD-74, 39 pp., doi:10.5065/D6C8277W.

Liu, H., G. Peters, and T. Foken, 2001: New equations for sonic temperature variance and buoyancy heat flux with an omnidirectional sonic anemometer. *Bound.-Layer Meteor.,* **100,** 459–468, doi:10.1023/A:1019207031397.

Lothon, M., and Coauthors, 2014: The BLLAST field experiment: Boundary-layer late afternoon and sunset turbulence. *Atmos. Chem. Phys. Discuss.,* **14,** 10 789–10 852, doi:10.5194/acpd-14-10789-2014.

Madgwick, S. O. H., 2010: An efficient orientation filter for inertial and inertial/magnetic sensor arrays. University of Bristol Rep., 32 pp.

Mansour, M., G. Kocer, C. Lenherr, N. Chokani, and R. Abhari, 2011: Seven-sensor fast-response probe for full-scale wind turbine flowfield measurements. *J. Eng. Gas Turbines Power,* **133,** 081601, doi:10.1115/1.4002781.

Marks, F. D. J., 2005: Recent results from NOAA's Hurricane Intensity Forecast Experiment (IFEX). *11th Symp. on Integrated Observing and Assimilation Systems for the Atmosphere, Oceans, and Land Surface (IOAS-AOLS),* Miami, FL, Amer. Meteor. Soc., 8.1. [Available online at https://ams.confex.com/ams/87ANNUAL/webprogram/Paper119567.html.]

Marques, F., L. M. F. Ribeiro, and V. Meles, 2013: Aerial sonic anemometry - preliminary results. *First Conf. of the Int. Society for Atmospheric Research Using Remotely-Piloted Aircraft,* Palma de Mallorca, Balearic Islands, Spain. [Available online at www.cost-uas.net/fileadmin/user_upload/infos/Meetings/Meeting_Palma_20120218/ISARRA_Conference/Poster_Session/poster_ASA_-_Aerial_Sonic_Anemometry_-_Preliminary_results.pdf.]

Martin, S., J. Bange, and F. Beyrich, 2010: Meteorological profiling of the lower troposphere using the research UAV "M^2AV Carolo." *Atmos. Meas. Tech. Discuss.,* **3,** 5179–5209, doi:10.5194/amtd-3-5179-2010.

Marwitz, J. D., 1972: The structure and motion of severe hailstorms. Part I: Supercell storms. *J. Appl. Meteor.,* **11,** 166–179, doi:10.1175/1520-0450(1972)011<0166:TSAMOS>2.0.CO;2.

Mayer, S., 2011: Application and improvement of the unmanned aerial system SUMO for atmospheric boundary layer studies. Ph.D. thesis, Geophysical Institute, University of Bergen, 24 pp.

——, G. Hattenberger, P. Brisset, M. Jonassen, and J. Reuder, 2012a: A 'no-flow-sensor' wind estimation algorithm for unmanned aerial systems. *Int. J. Micro Air Veh.,* **4,** 15–30, doi:10.1260/1756-8293.4.1.15.

——, M. O. Jonassen, A. Sandvik, and J. Reuder, 2012b: Profiling the Arctic stable boundary layer in Advent valley, Svalbard: Measurements and simulations. *Bound.-Layer Meteor.,* **143,** 507–526, doi:10.1007/s10546-012-9709-6.

——, A. Sandvik, M. O. Jonassen, and J. Reuder, 2012c: Atmospheric profiling with the UAS SUMO: A new perspective for the evaluation of fine-scale atmospheric models. *Meteor. Atmos. Phys.,* **116,** 15–26, doi:10.1007/s00703-010-0063-2.

Moore, R. J., S. Thurrowgood, and M. V. Srinivasan, 2012: Vision-only estimation of wind field strength and direction from an aerial platform. *2012 IEEE/RSJ International Conference on Intelligent Robots and Systems,* IEEE, 4544–4549.

Premerlani, W., and P. Bizard, 2009: Direction cosine matrix IMU: Theory. Gentlenav Doc., 30 pp. [Available online at http://gentlenav.googlecode.com/files/DCMDraft2.pdf.]

Quindlen, J., and J. Langelaan, 2013: Flush air data sensing for soaring-capable UAVs. *51st AIAA Aerospace Sciences Meeting Including the New Horizons Forum and Aerospace Exposition,* Grapevine, TX, American Institute of Aeronautics and Astronautics, AIAA 2013-1153, doi:10.2514/6.2013-1153.

Ramanathan, V., M. V. Ramana, G. Roberts, D. Kim, C. Corrigan, C. Chung, and D. Winker, 2007: Warming trends in Asia amplified by brown cloud solar absorption. *Nature,* **448,** 575–578, doi:10.1038/nature06019.

Reineman, B. D., L. Lenain, N. M. Statom, and W. K. Melville, 2013: Development and testing of instrumentation for UAV-based flux measurements within terrestrial and marine atmospheric boundary layers. *J. Atmos. Oceanic Technol.,* **30,** doi:10.1175/JTECH-D-12-00176.1.

Reuder, J., P. Brisset, M. Jonassen, M. Müller, and S. Mayer, 2009: The small unmanned meteorological observer SUMO: A new tool for atmospheric boundary layer research. *Meteor. Z.,* **18,** 141–147, doi:10.1127/0941-2948/2009/0363.

——, M. O. Jonassen, and H. Ãlafsson, 2012: The small unmanned meteorological observer SUMO: Recent developments and applications of a micro-UAS for atmospheric boundary layer research. *Acta Geophys.,* **60,** 1454–1473, doi:10.2478/s11600-012-0042-8.

Roadman, J. M., J. Elston, B. Argrow, and E. Frew, 2012: Performance of the electric-powered tempest UAS in supercell storms. *J. Aircraft,* **49,** 1821–1830, doi:10.2514/1.C031655.

Rogers, K., and A. Finn, 2013: Three-dimensional UAV-based atmospheric tomography. *J. Atmos. Oceanic Technol.,* **30,** 336–344, doi:10.1175/JTECH-D-12-00036.1.

Savage, P. G., 1998: Strapdown inertial navigation integration algorithm design part 1: Attitude algorithms. *J. Guid. Control Dyn.,* **21,** 19–28, doi:10.2514/2.4228.

Schotanus, P., F. T. M. Nieuwstadt, and H. A. R. De Bruin, 1983: Temperature measurement with a sonic anemometer and its application to heat and moisture fluxes. *Bound.-Layer Meteor.,* **26,** 81–93, doi:10.1007/BF00164332.

Shuqing, M., C. Hongbin, W. Gai, P. Yi, and L. Qiang, 2004: A miniature robotic plane meteorological sounding system. *Adv. Atmos. Sci.,* **21,** 890–896, doi:10.1007/BF02915591.

Singha, A., and R. Sadr, 2013: In situ calibration of four-wire hot-wire probes for atmospheric measurement. *Exp. Therm. Fluid Sci.,* **44,** 82–89, doi:10.1016/j.expthermflusci.2012.05.016.

Smit, H., R. Kivi, H. Vömel, and A. Paukkunen, 2013: Thin film capacitive sensors. *Monitoring Atmospheric Water Vapour,* Springer, 11–38.

Soddell, J., K. McGuffie, and G. Holland, 2004: Intercomparison of atmospheric soundings from the aerosonde and radiosonde. *J. Appl. Meteor.,* **43,** 1260–1269, doi:10.1175/1520-0450(2004)043<1260:IOASFT>2.0.CO;2.

Spieß, T., 2006: A contribution to turbulence measurements with autonomous micro aerial vehicles. Ph.D. thesis, Braunshweig University of Technology, 120 pp.

——, and J. Bange, 2006: Comparison of 'M2AV' unmanned airborne meteorological measurements with remote sensing and the Helipod. *17th Symp. on Boundary Layers and Turbulence,* San Diego, CA, Amer. Meteor. Soc., 7.4. [Available online at https://ams.confex.com/ams/BLTAgFBioA/techprogram/paper_109559.htm.]

——, ——, M. Buschmann, and P. Vörsmann, 2007: First application of the meteorological mini-UAV 'M^2AV.' *Meteor. Z.,* **16,** 159–169, doi:10.1127/0941-2948/2007/0195.

Stainback, P., and K. Nagabushana, 1993: Review of hot-wire anemometry techniques and the range of their applicability for various flows. *Electron. J. Fluid Eng. Trans. ASME,* **167,** 1–54.

Storvold, R., S. Solbø, J. Burkhart, W. Bogren, C. Pedersen, S. Forsstrom, and S. Gerland, 2011: Atmospheric effects on UAS based spectral remote sensing reflectance measurements of snow surfaces. *2011 Fall Meeting,* San Francisco, CA, Amer. Geophys. Union, Abstract C41D-0435.

Tarbert, B., and T. Wierzbanowski, 2009: Small unmanned aircraft system aviation rulemaking committee: Comprehensive set of recommendations for sUAS regulatory development. U.S. Department of Transportation Tech. Rep., 9 pp.

Telionis, D., Y. Yang, and O. Redinioti, 2009: Recent developments in multi-hole probe (MHP) technology. *Proc. 20th Int. Congress of Mechanical Engineering (COBEM2009),* Gramado, RS, Brazil, ABCM, COBO9-3415. [Available online at http://www.abcm.org.br/pt/wp-content/anais/cobem/2009/pdf/COB09-3415.pdf.]

Tjernström, M., and C. A. Friehe, 1991: Analysis of a radome air-motion system on a twin-jet aircraft for boundary-layer research. *J. Atmos. Oceanic Technol.,* **8,** 19–40, doi:10.1175/1520-0426(1991)008<0019:AOARAM>2.0.CO;2.

U.S. House of Representatives, 2012: FAA modernization and reform act of 2012. Conference Rep. 112–381, U.S. Government, 296 pp. [Available online at http://www.gpo.gov/fdsys/pkg/CRPT-112hrpt381/pdf/CRPT-112hrpt381.pdf.]

Van den Kroonenberg, A. C., T. Martin, M. Buschmann, J. Bange, and P. Vörsmann, 2008a: Measuring the wind vector using the autonomous mini aerial vehicle M^2AV. *J. Atmos. Oceanic Technol.,* **25,** 1969–1982, doi:10.1175/2008JTECHA1114.1.

——, T. Spieß, and J. Bange, 2008b: First wind measurements with the meteorological UAV 'M^2AV Carolo.' *18th Symp. on Boundary Layers and Turbulence,* Stockholm, Sweden, Amer. Meteor. Soc., 6B.4. [Available online at https://ams.confex.com/ams/18BLT/techprogram/paper_139842.htm.]

van Graas, F., and J. L. Farrell, 2001: GPS/INS—A very different way. *Proceedings of the 57th Annual Meeting of the Institute of Navigation,* ION, 715–721.

van Vuren, R. J., 1981: Model aircraft operating standards. U.S. Department of Transportation Advisory Circular AC 91-57. [Available online at http://www.faa.gov/documentLibrary/media/Advisory_Circular/91-57.pdf.]

Vörsmann, P., C. Kaschwich, T. Krüger, P. Schnetter, and C.-S. Wilkens, 2012: MEMS based integrated navigation systems for adaptive flight control of unmanned aircraft—State of the art and future developments. *Gyroscopy Navig.,* **3,** 235–244, doi:10.1134/S2075108712040116.

Wildmann, N., 2011: Measurement of the structures and processes in the atmospheric boundary layer during the late-afternoon transition using the recently developed research UAV 'MASC,' including the comparison with other UAV organised in COST action ES 0802. BLLAST Rep., 8 pp. [Available online at http://bllast.sedoo.fr/documents/reports/UAS/BLLAST_UAS_COST-es0802_report_20110802_Wildmann.pdf.]

——, M. Mauz, and J. Bange, 2013: Two fast temperature sensors for probing of the atmospheric boundary layer using small remotely piloted aircraft (RPA). *Atmos. Meas. Tech.,* **6,** 2101–2113, doi:10.5194/amt-6-2101-2013.